IEEE Access
Multidisciplinary | Rapid Review | Open Access Journal

Received January 19, 2021, accepted February 6, 2021, date of publication February 23, 2021, date of current version March 25, 2021.

Digital Object Identifier 10.1109/ACCESS.2021.3061533

Enhancement of Contour Smoothness by Substitution of Interpolated Sub-Pixel Points for Edge Pixels

TIAN-HU LIU, GUI-QI LI, XIANG-NING NIE, HONG-JUN WANG, DI ZHANG, JIN-MENG WU, AND WEI LIU

College of Engineering, South China Agricultural University, Guangzhou 510642, China

Corresponding author: Hong-Jun Wang (xtwhj@scau.edu.cn)

This work was supported in part by the National Key Research and Development Program of China under Grant 2018YFD0101001, and in part by the Guangdong Science and Technology Plan Project under Grant 2017A010102024 and Grant 2017A020208052.

ABSTRACT This study designed a sub-pixel precision edge detecting algorithm to enhance contour smoothness. First, the coordinate value of RGB pixel is projected on the space line of R=G=B to obtain gray image. Then, pixel edges are located using a Canny detector. Next, the edge width is thinned to a single pixel using a morphological thinning operation. Finally, sub-pixel-level smooth contours are extracted by interpolation. In this sub-pixel level contour extraction process, a Single-Pixel-Multi-Point interpolation method was developed to enhance edge smoothness and obtain high precision in edge estimation. This method divides edges in a 3×3 pixels block into nine arrangement modes. According to the arrangement of the eight neighborhoods of a centered edge pixel, different locations of interpolated sub-pixel points are calculated by interpolation with Bezier curves. For symmetrically arranged linear edge pixels, this method can be used to determine the exact contour. Experimental results showed that the proposed algorithm can improve the smoothness of image edge contour. As the curvature of the edge increases, the maximum systematic error will increase. For the edge pixel centered in the 3×3 pixels block and two pixels located at the corner of one side, the max systematic error is 0.5 pixel. For two edge pixels aligned in a single row or column with one located at a corner, the max systematic error is 0.25 pixel.

INDEX TERMS Computer vision, image segmentation, sub-pixel contour detection.

I. INTRODUCTION

Pixel level edge detectors are unable to accurately detect a smooth contour. In this study, a sub-pixel precision algorithm was developed to enhance contour smoothness. Edge detection is an important aspect of image processing. All thresholding operations must be performed at pixel-level precision. Some applications require even higher accuracy than a pixel grid. Therefore, traditional methods of pixel level detection have been improved to achieve sub-pixel level performance. In 1973, Hueckel [1] first proposed the concept of sub-pixel detection. Subsequently, many different methods of sub-pixel edge detection have been described, including moment-based, fitting-based and interpolation-based methods.

The associate editor coordinating the review of this manuscript and approving it for publication was Yonghong Peng.

Moment-based methods are insensitive to noise. Tabatabai and Mitchell [2] reported a moment-based method to locate edges in digital data to sub-pixel values. Lyvers *et al.* [3] used six moments to measure sub-pixels. Ghosal and Mehrotra [4] applied Zernike orthogonal moments (ZOM) in sub-pixel edge detection. ZOM are invariant under rotation, but ZOM-based methods cannot accurately detect small objects [5]. Balasundaram and Ratnam [6] used the grey level invariant moment to detect the edge of the surface contour to sub-pixel accuracy. Adapa *et al.* [7] proposed a new supervised method for blood vessel segmentation using Zernike moment-based shape descriptors. Qu *et al.* [8] combined a ZOM operator with a Sobel operator for edge detection. In that method, all probable edge points are first detected using the Sobel operator, and then the ZOM operator is used to precisely locate the edge. However, this method has low accuracy for the detection of curvature. Xie *et al.* [9] proposed

an improved sub-pixel edge detection algorithm combining coarse and precise location, the proposed algorithm effectively improves the detection efficiency and the detection accuracy. Wang *et al.* [10] proposed a SPM method with point constraints into SPM to increase map accuracy. Lee *et al.* [11] proposed a novel sub-pixel level edge detection algorithm for micron scale CD measurement with active contour method and fast pixel resampling. Kaur and Singh[12] employed Pseudo Zernike moments for sub-pixel edge detection, with significantly better results than methods based on ZOM and OFMMs. Wei and Zhao[13] applied ZOM to relocate the edge of a micro-size part at the sub-pixel level. Sun *et al.* [14] combined a gray moments operator with a smoothing spline algorithm for edge detection, but moment-based methods require high computational cost.

In fitting-based methods, high precision edge position is determined by fitting the gray value according to the least-squared-error. Sun *et al.* [15] used Sobel operator and cubic surface fitting method to determine the normal direction of edge in subpixel edge detection. Wang [16] combined Randomized Hough Transform and subpixel circle fitting in circle extraction. Wei *et al.* [17] used Sobel operator and the least square method to obtain sub-pixel edge position. Li and Zhang [18] used an improved Canny algorithm and linear fitting method in edge detection.

Interpolation-based techniques determine the sub-pixel edge by interpolating the gray value or its derivatives. Jensen and Anastassiou [19] proposed sub-pixel edge localization by interpolation. Hermosilla *et al.* [20] detected the sub-pixel edge by non-linear fourth-order image interpolation. Pap and Zou [21] described a similar method. Shi *et al.* [22] detected the sub-pixel linear edge based on the first derivative. Chen *et al.* [23] presents a sub-pixel image edge detection method based on the cubic B-spline curve interpolation and the wavelet transform. Sánchez [24] proposed an image edge detector by incorporating the main ideas of the classic Canny and Devernay algorithms.

From a theoretical point of view, the approach we propose here is an interpolation-based sub-pixel edge detection method. Traditional interpolation-based methods relocate the pixel by interpolating the gray gradient using methods such as Lagrange interpolation, polynomial interpolation and radial basis function interpolation. Technically, this method differs from those traditional interpolation-based methods, because in addition to relocating the pixel, it replaces the edge pixel with several interpolated sub-pixel points to increase the smoothness of contours. This paper is organized as follows: in section 2, we introduce the algorithm, experiments and discussion are presented in section 3 and section 4 the conclusion.

II. ALGORITHM

A. ALGORITHM DESCRIPTION

The main processing flow of the algorithm is shown in Fig.1. The algorithm includes four steps. First, Through

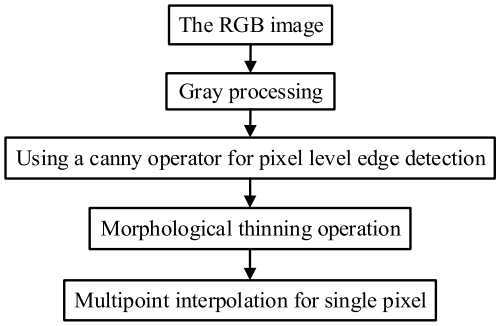

FIGURE 1. The main processing flow of the sub-pixel contour extraction algorithm.

the mapping principle of R, G and B three-dimensional space cartesian coordinate system, the coordinate value of RGB pixel is projected on the space line of R=G=B to obtain gray image. The implementation is achieved by

$$\text{Gray} = 0.29900 * \text{R} + 0.58700 * \text{G} + 0.11400 * \text{B} \quad (1)$$

Then, pixel edges are detected using a Canny detector. Third, the edge width is thinned to a single pixel by application of a morphological thinning operation. Finally, the contour smoothness is enhanced by substitution of interpolated sub-pixel points for each edge pixel according to the eight neighborhood edge pixels arrangement modes in a 3×3 pixels block. This paper focuses on edge detection and the sub-pixel contour extraction algorithm.

B. PIXEL LEVEL EDGE DETECTION USING A CANNY OPERATOR

The best way to robustly describe the boundaries of objects is by considering them as edges in the image [25]. Assuming that the gray values in the object and background are constant and the image is continuous, edges in real images are locations where the gray values change significantly. The first derivative of the gray values at edge points differs significantly from 0. In digital image processing, derivative operation is replaced by differential operation. The Canny operator selects a Gaussian filter to smooth the image, and then uses non-maxima suppression to obtain the edge of the image [26].

The first step of the Canny operator is to smooth the image with a Gaussian smoothing filter. The Gaussian smoothing filter can effectively suppress normally distributed noises. The smoothing algorithm is expressed as

$$G(x, y) = f(x, y) * H(x, y, \delta) \quad (2)$$

where $f(x, y) f(x, y)$ represents the original image, f(x, y)$G(x, y)$ is the smoothed image, and $H(x, y, \delta)$ is the Gaussian filter, which is given by

$$H(x, y, \delta) = \frac{1}{2\pi\delta^2} \exp(-\frac{x^2 + y^2}{2\delta^2}) \quad (3)$$

where δ is the standard deviation.

With the increase of the standard deviation δ, filtered images are more and more blurred. This is because an increase in δ increases the effect scope of the Gaussian filter on the local image. However, an increase in δ results in increased smoothness of an image. In this study, a Gaussian filter of as expressed as Eq. (4) is used.

$$\begin{vmatrix} a_1 & a_2 & a_3 \\ a_4 & a_5 & a_6 \\ a_7 & a_8 & a_9 \end{vmatrix} = \frac{1}{13.3156} \begin{vmatrix} 1.0002 & 1.6490 & 1.0002 \\ 1.4690 & 2.7188 & 1.6490 \\ 1.0002 & 1.6490 & 1.0002 \end{vmatrix} \tag{4}$$

The second step is to compute the magnitude of gradient and its orientation. The gradient of a pixel (x, y) is a vector which can be expressed as

$$\nabla f(x, y) = (\frac{\partial f}{\partial x}, \frac{\partial f}{\partial y}) \tag{5}$$

where, $\partial f/\partial x$ and ∂f$/\partial$x $\partial f/\partial x$ $\partial f/\partial y$ are partial derivatives in the x and y directions, and represent the change rate of the gray value in x and y directions. The magnitude of gradient is given by

$$\|\nabla f(x, y)\| = \sqrt{(\frac{\partial f}{\partial x})^2 + (\frac{\partial f}{\partial y})^2} \tag{6}$$

The differential operations $\nabla_x f(x, y)$ and $\nabla_y f(x, y)$ are used to approximately replace the derivative operations $\partial f/\partial x$ and $\partial f/\partial y$. The differences of consecutive gray values on the profile are not symmetric, so a symmetric approach is applied to compute the first partial derivatives, which is given by

$$\nabla_x f(x, y) = \frac{1}{2}[f(x + 1, y) - f(x - 1, y)] \tag{7}$$

and

$$\nabla_y f(x, y) = \frac{1}{2}[f(x, y + 1) - f(x, y - 1)] \tag{8}$$

The above methods to compute the first x and y direction partial derivatives can then be regarded as convolution masks $\frac{1}{2}\left|1\ 0\ -1\right|\left|1\ 0\ -1\right|/2$ and $\left|1\ 0\ -1\right|^T/2\frac{1}{2}\left|1\ 0\ -1\right|^{\mathrm{T}}$.

Substituting differential operations for derivative operations, the magnitude of gradient can be transformed to Eq. (9).

$$\|\nabla f(x, y)\| = [\nabla_x f(x, y)^2 + \nabla_y f(x, y)^2]^{\frac{1}{2}} \tag{9}$$

The direction of the gradient is given by

$$\theta(x, y) = \arctan \frac{\nabla_y f(x, y)}{\nabla_x f(x, y)} \tag{10}$$

The third step is to apply non-maxima suppression to the magnitude of the gradient. Next, the double thresholding algorithm is applied to detect and link edges. Thresholds $T_1 = 30$ and $T_2 = 60$ can be applied to obtain two edge images $N_1(i, j)$ and $N_2(i, j)$. $T_2 = 60$ is used to identify each line segment, and $T_1 = 30$ is used to extend the two directions of the line segment to find the edge of the fracture and to connect the edges.

In addition to the Canny operator, Sobel [27], Laplace [28], Roberts [29], Prewitt [30], and Marr-Hildreth [31]operators

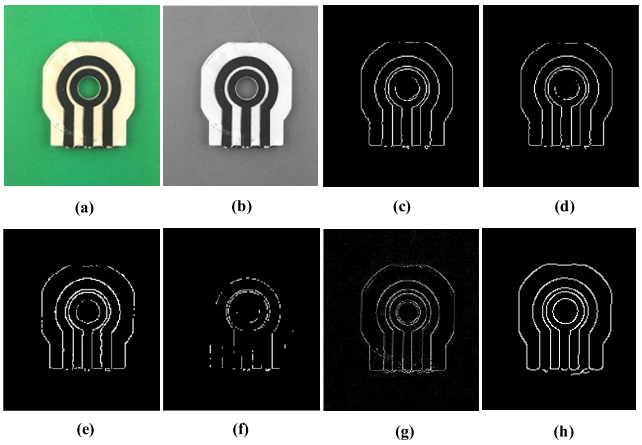

FIGURE 2. Segmented pixel edges using different operators. (a) The original image, (b) After rgb2gray color space transformation, (c) Sobel operator, (d) Prewitt operator, (e) Roberts operator, (f) Marr-Hildreth operator, (g) Laplace operator, and (h) Canny operator.

are commonly used as edge-detecting operators. Fig. 2 compares the segmentation of edge images using those operators. For the convenience of comparison, the parameters of threshold and Gaussian standard deviation are the same in each program. The positioning accuracy of the Sobel and Prewitt operators is comparatively low. The Laplace operator is highly sensitive to noise. Although the Roberts operator is very accurate for edge segmentation, it is also sensitive to noise. The Marr-Hildreth operator is sensitive to threshold value and Gaussian standard deviation size. Overall, the Canny operator is best suited for the segmentation of edges in this study.

C. MORPHOLOGICAL THINNING OPERATION

Sometimes, the edges segmented by the Canny operator may be more than 1 pixel in width. A thinning process can be applied to remove pixels from the original edges, while keeping the original shape unchanged. If the removal of a pixel will not increase the connected component, then that pixel can be removed from the edge. Inside pixels, isolated pixels, and the end pixel of a line should not be removed. The edge width is thinned to a single pixel using a morphological thinning operation. Comparison before and after the morphological refinement operation is shown in Fig. 3. In this figure, three sets of processing block diagrams of 3 × 3 pixel blocks are marked.

D. SINGLE-PIXEL-MULTI-POINT INTERPOLATION

We propose a method to substitute the interpolated sub-pixel multipoint for the edge pixel according to the eight neighborhood edge pixel arrangement modes in a 3 × 3 pixels block, to enhance edge smoothness and obtain high precision for edge estimation. This method is named as the Single-Pixel-Multi-Point interpolation. The flow of the interpolation algorithm can be represented in Fig. 4.

After morphology refinement, there are less than six edge pixels in a thinned 3 × 3 pixels block. The arrangement

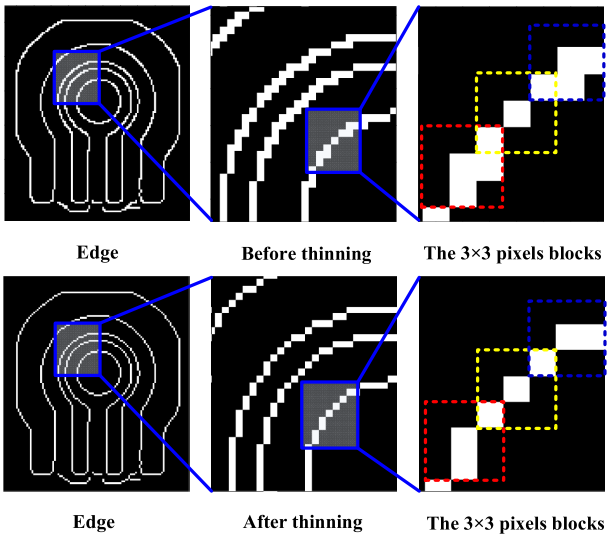

FIGURE 3. Before and after applying thinning operation.

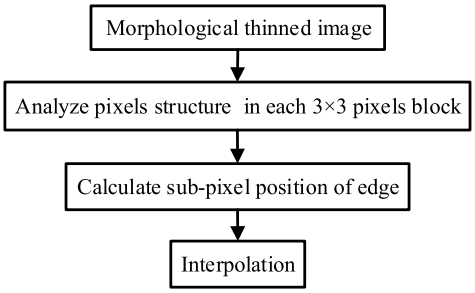

FIGURE 4. Process of the interpolation algorithm.

modes of the eight neighborhood edge pixels for a thinned edge pixel can be divided into nine kinds, including one for an isolated single pixel edge, two for two-pixel edges, three for three-pixel edges, two for four-pixel edges, and one for five-pixel edge, as shown in Fig.5. The black pixel in the figure represents the edge pixel after morphology refinement. The isolated single pixel edge is taken as noise, and will be removed. The centered edge pixel of a two-pixel edge is the end pixel of a line or curve. The coordinates of the interpolated sub-pixel points are the same as that for three-pixel edges. Those three kinds of arrangement modes for three-pixel edges include symmetrical, V-type, and L-type. Multiple points are interpolated to replace a certain edge pixel (i, j) according to the arrangement of the neighborhood edge pixels in a 3 × 3 pixels block. In this subsection, such multipoint edge interpolation method will be fully discussed. Single point and three-point interpolation methods are presented, but interpolation methods with more points could be applied.

1) INTERPOLATION METHOD OF SYMMETRICAL ALIGNING THREE PIXELS EDGES

The contour of symmetrical alignment of a three-pixel edge is a line. There are four such arrangement modes, as shown in

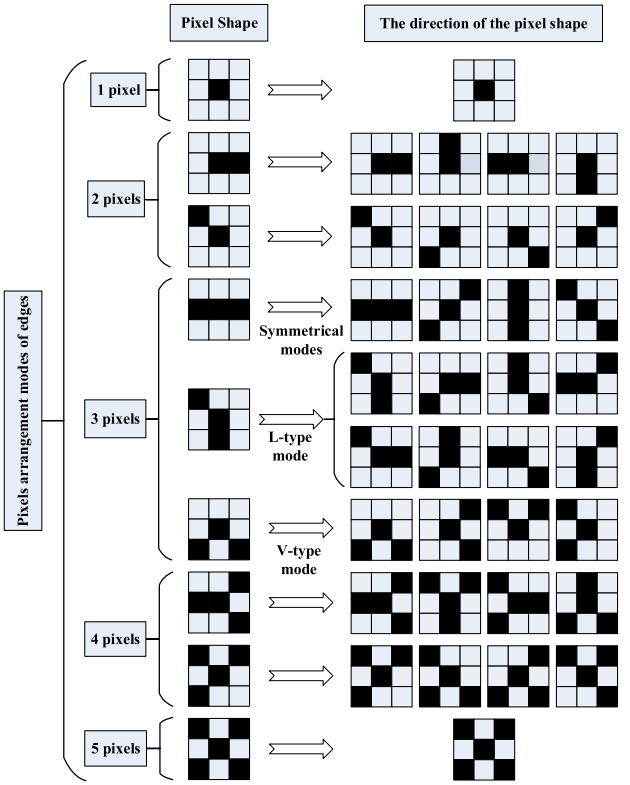

FIGURE 5. Arrangement modes of the eight neighborhood edge pixels for a thinned edge pixel.

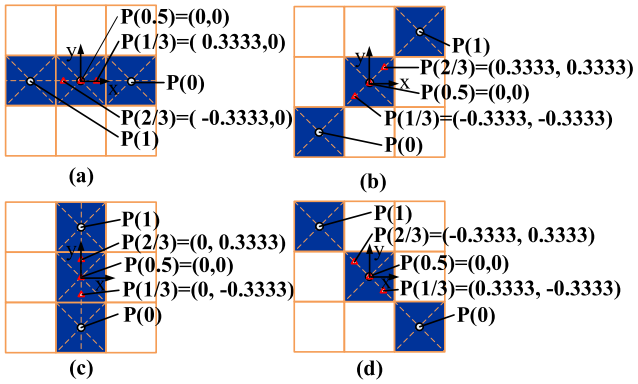

FIGURE 6. Symmetrical aligned three-pixel edges, (a) in 0°, (b) in 45°, (c) in 90°, and (d) in 135°.

Fig. 6. In these 4 arrangement modes, the edge is represented by a straight-line equation. It is unnecessary to adjust the position of an edge pixel to obtain a smooth sub-pixel contour. The sub-pixel points of the contour are located on that straight line. Our method to obtain the sub-pixel contour is to insert some points on that straight line and connect them. The straight-line equation in Fig. 6(a) is expressed by $y = 0$, where the coordinate system is centered at the edge pixel (i, j). That center pixel is replaced by sub-pixel points (−0.3333, 0), (0, 0), and (0.3333, 0). Similarly, in the case presented in Fig. 3(b), the edge pixel (i, j) is replaced by sub-pixel points (−0.3333, −0.3333), (0, 0), and (0.3333, 0.3333). For the

case presented in Fig. 3(c), the edge pixel (i, j) is replaced by sub-pixel points (0, −0.3333), (0, 0), and (0, 0.3333). For the case presented in Fig. 3(d), the edge pixel (i, j) is replaced by sub-pixel points (−0.3333, 0.3333), (0, 0), and (0.3333, −0.3333).

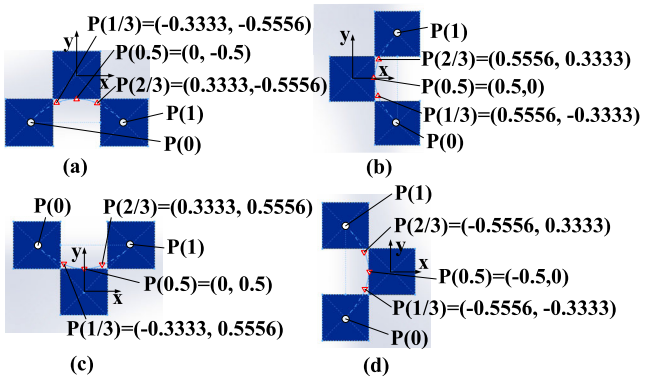

FIGURE 7. V-type edge pixels arrangement modes, (a) in 0°, (b) in 90°, (c) in 180°, and (d) in 270°.

2) INTERPOLATION METHOD FOR V-TYPE ARRANGEMENT MODES

In the V-type edge pixel arrangement mode, one edge pixel is in the center and two edge pixels are located at the two corners of one side. There are four such edge pixel arrangement modes in a 3 × 3 pixels block, as shown in Fig. 7. In these cases, the smooth sub-pixel contour can be represented by a curve equation. In this method, Bezier curves are used to describe the sub-pixel contour. In the case illustrated in Fig. 7(a), the edge pixel (i, j) is centered in the 3 × 3 pixels block, and edge pixels (i−1, j−1) and (i+1, j−1) are located at the two corners of the bottom side. We assume that the coordinates of pixels (i, j), (i−1, j−1), and (i+1, j−1) are (0, 0), (−1, −1), and (1, −1), respectively. The starting point $P(0)$ of the Bezier curves is (−1, −1) and the end point $P(1)$ is (1, −1). Point (0, 0) is the pole. The equation of a Bezier curves is given by [32]

$$BEZ_{i,n}(t) = C_n^i t^i (1-t)^{n-i} = \frac{n!}{i!(n-i)!} t^i (1-t)^{n-1}, \quad t = [0, 1] \qquad (11)$$

For a three-point Bezier curve, n = 2. Square Bezier curves are expressed as

$$P(t) = \sum_{i=0}^{2} P_i \cdot BEZ_{i,2}(t) = (1-t)^2 P_0 + 2t(1-t)P_1 + t^2 P_2, \quad t = [0, 1] \qquad (12)$$

or

$$P(t) = \begin{bmatrix} t^2 & t & 1 \end{bmatrix} \begin{bmatrix} 1 & -2 & 1 \\ -2 & 2 & 0 \\ 1 & 0 & 0 \end{bmatrix} \begin{bmatrix} P_0 \\ P_1 \\ P_2 \end{bmatrix}, \quad t = [0, 1] \qquad (13)$$

where P_i is the control vertex, $i \in \{0, 1, 2\}$.

The coordinates of three interpolated sub-pixel points of a certain edge pixel (i, j) are calculated using equation (12). The coordinates of the first interpolated point are

$$P\left(\frac{1}{3}\right) = \begin{bmatrix} (\frac{1}{3})^2 & \frac{1}{3} & 1 \end{bmatrix} \begin{bmatrix} 1 & -2 & 1 \\ -2 & 2 & 0 \\ 1 & 0 & 0 \end{bmatrix} \times \begin{bmatrix} -1 & -1 \\ 0 & 0 \\ 1 & -1 \end{bmatrix} = \begin{bmatrix} -0.3333 & -0.5556 \end{bmatrix} \qquad (14)$$

The coordinates of the second interpolated point are

$$P(\frac{1}{2}) = \begin{bmatrix} (\frac{1}{2})^2 & \frac{1}{2} & 1 \end{bmatrix} \begin{bmatrix} 1 & -2 & 1 \\ -2 & 2 & 0 \\ 1 & 0 & 0 \end{bmatrix} \begin{bmatrix} -1 & -1 \\ 0 & 0 \\ 1 & -1 \end{bmatrix} = \begin{bmatrix} 0 & -0.5 \end{bmatrix} \qquad (15)$$

The coordinates of the third interpolated point are

$$P\left(\frac{2}{3}\right) = \begin{bmatrix} (\frac{2}{3})^2 & \frac{2}{3} & 1 \end{bmatrix} \begin{bmatrix} 1 & -2 & 1 \\ -2 & 2 & 0 \\ 1 & 0 & 0 \end{bmatrix} \times \begin{bmatrix} -1 & -1 \\ 0 & 0 \\ 1 & -1 \end{bmatrix} = \begin{bmatrix} 0.3333 & -0.5556 \end{bmatrix} \qquad (16)$$

Similar interpolation method is applied in the cases shown in Figs. 7(b), (c) and (d). The interpolation coordinates of four different combinations of V-type arrangement modes directions are also shown in Fig. 7.

3) INTERPOLATION METHOD FOR L-TYPE ARRANGEMENT MODES

In the L-type edge pixels arrangement modes, two edge pixels are aligned in one row or one column, and one edge pixel is located at one corner. There are eight such edge pixels arrangement modes in a 3 × 3 pixels block, as shown in Fig. 8. In these cases, we also use Bezier curves to describe the sub-pixel smooth contour. Similarly, the edge pixel (i, j) can be replaced by three interpolated sub-pixel points.

In the case shown in Fig.8(a), the edge pixel (i, j) is centered in the 3 × 3 pixels block. Edge pixels (i, j) and (i, j−1) align in one column. Edge pixel (i−1, j+1) is located at the left top corner. Assuming that the coordinates of pixels (i, j), (i, j−1), and (i−1, j+1) are respectively (0, 0), (0, −1), and (−1, 1), three sub-pixel points of a certain edge pixel (i, j) are interpolated using equation (12) and the locations are (−0.1111, −0.3333), (−0.25, 0), and (−0.4444, 0.3333). Similar interpolation method is applied in the cases shown in Figs.8(b)-(h). For example, in the case shown in Fig. 8(e), three interpolated sub-pixel points of the edge pixel (i, j) are (−0.3333, 0.4444), (0, 0.25), and (0.3333, 0.1111).

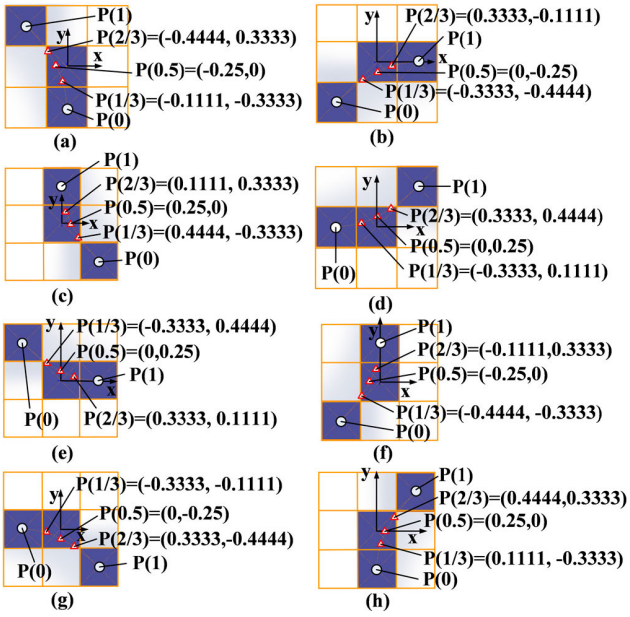

FIGURE 8. L-type arrangement modes, (a) in 0°, (b) in 90°, (c) in 180°, and (d) in 270°, an another L-type arrangement modes, (e) in 0°, (f) in 90°, (g) in 180°, and (h) in 270°.

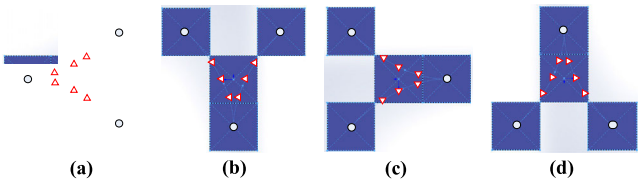

FIGURE 9. Four pixels edge of two edge pixels aligned in one row or one column and two edge pixels located at two corners, (a) in 0°, (b) in 90°, (c) in 180°, and (d) in 270°.

4) INTERPOLATION METHOD FOR FOUR-PIXEL EDGES

There are two kinds of shapes for a four-pixel edge. The first one is for two edge pixels aligned in one row or column and two edge pixels located at two corners. Fig. 6 shows the four possible directions. This shape can be interpreted as two L-type arrangement modes folded together. For example, image in Fig. 9(a) can be considered as images in Figs. 8(d) and (g) folded together. The sub-pixel points of the smooth contour can be obtained by folding the interpolated results of Figs.8(d) and (g) together.

In the second kind of shape, there are three edge pixels located at three corners. This can be considered as two V-type arrangement modes folded together. For example, Fig. 10(a) can be considered as Figs. 7(c) and (d) folded together. The sub-pixel points of the smooth contour can be obtained by folding the interpolated results of Figs. 7(c) and (d) together.

5) INTERPOLATION METHOD FOR A FIVE-PIXEL EDGE

There is only one shape for a five-pixel edge in a thinned 3×3 pixels block, in which four edge pixels are located at the four corners of the 3×3 pixels block. This kind of edge

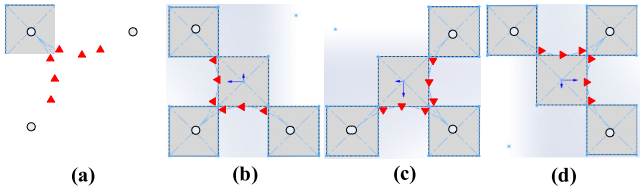

FIGURE 10. Four pixels edge of three pixels located at three corners, (a) in 0°, (b) in 90°, (c) in 180°, and (d) in 270°.

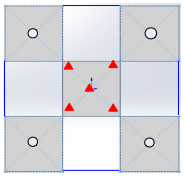

FIGURE 11. Interpolated sub-pixel points for five-pixel edges in a thinned 3×3 pixels block.

pixel arrangement mode can be visualized as the images in Figs. 6(b) and (d) folded together. Thus, the sub-pixel points of the smooth contour can be obtained by folding the interpolated results of Figs. 6(b) and (d) together. Fig. 11 illustrates the interpolated sub-pixel points for this case using red triangles.

III. EXPERIMENTS AND DISCUSSION

A. EXPERIMENTS USING REAL IMAGES

A ceramic substrate thick film printing resistor prints carbon and metal paste onto a substrate ceramic using a thick film printing process. The printed carbon paste forms a resistor that is matched with a small size electric brush to form a sliding rheostat. This can then be used as a core component for durable angle sensors. The precision of printed film is a key determinant of the accuracy of this kind of angle sensor. Pixel level edge detectors are unable to detect an accurate smooth contour for a ceramic substrate thick film printing resistor. In the experiment process, above algorithm is used to detect the sub-pixel contour of several ceramic substrate thick film printing resistors. In addition, this algorithm is applied to two additional examples to find the sub-pixel contour.

A machine vision system was developed to capture images of a ceramic substrate thick film printing resistor. This system consists of a test box, a light source, a CCD sensor, a USB based image grabbing card, and a Lenovo ThinkPad PC. The CCD sensor is a DCL200 (made by Hua-qi Digital Lab Inc.). The light source includes six 12W fluorescent lamps. The CCD sensor and the light source are installed on three sheets. MATLAB 2016a (The Mathworks, Inc.) was used to compute the coordinates of interpolated points.

An experiment was performed on a ceramic substrate thick film printing resistor. This method was applied for detection of pixel edges and sub-pixel contours by interpolating one point, or interpolating three points. Fig. 12 shows the pixel edges with the gradient vector superimposed on the initial image after morphological thinning. The contour of the

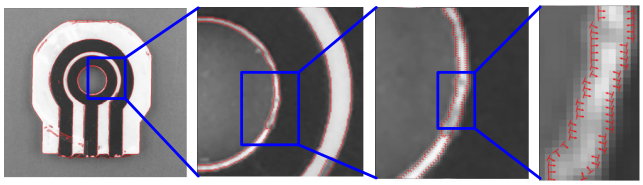

FIGURE 12. Thinned pixel level edge with gradient vector superimposed on the initial image.

ceramic substrate thick film printing resistor is extracted in the image but the edges are discrete only at the pixel level.

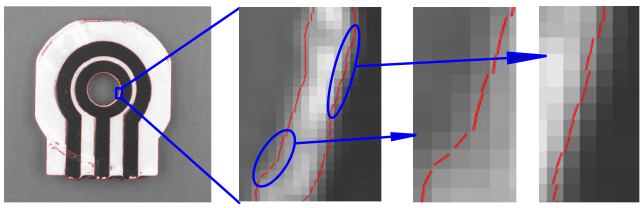

FIGURE 13. Detected sub-pixel contours by interpolating one point with gradient vector superimposed on the initial image.

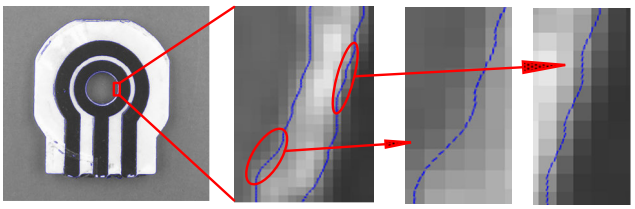

FIGURE 14. Detected sub-pixel contours by interpolating three points with gradient vector superimposed on the initial image.

Figs. 13 and 14 show the sub-pixel contours with a gradient vector superimposed on the initial image by interpolating one point and by interpolating three sub-pixel points, respectively. In Figs. 13 and 14, several zooms are used to compare contours extracted using our technique, and it's clear that the contours presented in Fig. 14 are visually smoother than those in Fig. 13. Two additional examples of this approach by interpolating three points are shown in Fig. 15, where (a), (b), (c) and (d) shows cases of detected sub-pixel contours of car engine gasket; (e), (f), (g) and (h) shows a sub-pixel contours of a chip circuit board. Fig.15 (c) and (g) indicated that the smoothness of edge contour was improved by interpolating one point into each edge pixel. The detected subpixel edge contour in Fig.15 (d) and (h) is even smoother than Fig.15 (c) and (g). Above comparison demonstrated that compared with no interpolation and interpolation of one point, three points interpolated edge is the smoothest.

Unlike moment-based Methods [3, 4, 8], no moment computation is required in our method. Additionally, the computational cost of this approach is low. Most existing interpolation-based methods relocate pixels on the edge according to the interpolated gray gradient. Here we use the centered edge pixel (i, j) as the pole point in the interpolation

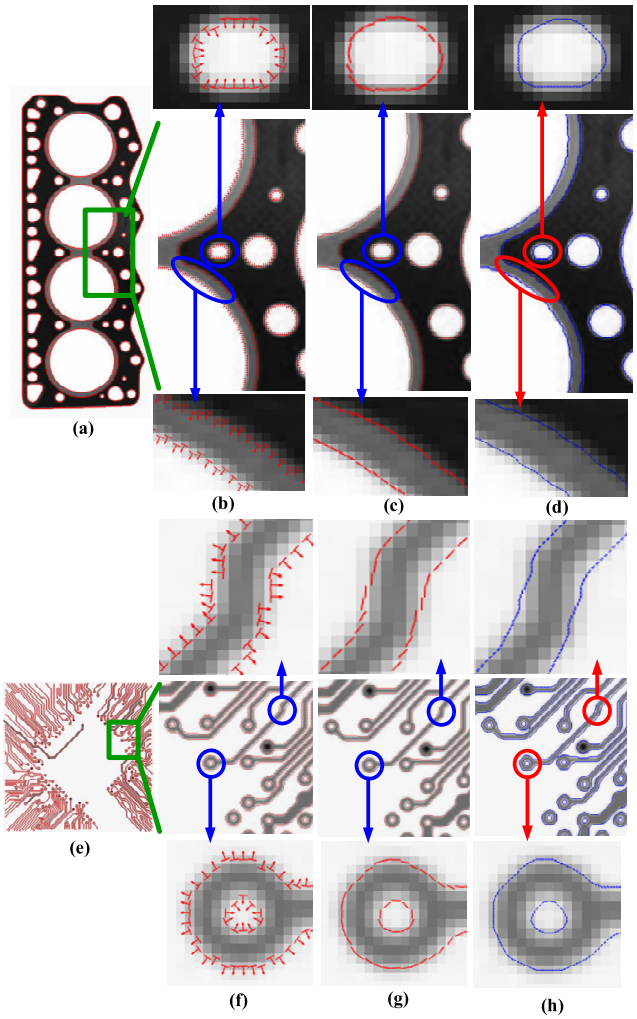

FIGURE 15. Other two cases of detection, (a) is a car engine gasket image, (b) gradient vector of (a), (c) interpolated one point, (d) interpolated three points; (e) a chip circuit board image, (f) gradient vector of (e), (g) interpolated one point, (h) interpolated three points.

process, and then perform relocation based on the assumption that the edge is smooth. This method substitutes several sub-pixel points for every edge pixel to enhance the smoothness of contours. To the best of our knowledge, this is the first attempt of this strategy for enhanced contour smoothness.

B. COMPARATIVE ANALYSIS OF APPLICATION AND PERFORMANCE OF DIFFERENT ALGORITHMS

Fig.15 has shown the comparison and analysis of the improved algorithm for sub-pixel edge smoothness optimization. In order to verify the effectiveness and advancement of the proposed algorithm, comparative experiments on the detection accuracy and detection time of different algorithms were conducted here.

1) COMPARATIVE ANALYSIS OF DETECTION ACCURACY

This set of experiments is to detect the accuracy of the pixel edge. First, use the MATLAB 2016a tool to

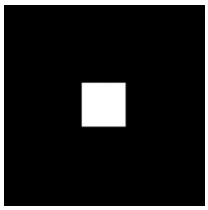

FIGURE 16. Artificial image.

TABLE 1. Artificial image sub-pixel edge coordinate.

Actual	Canny	Interpolate one point	Interpolate three points
(99.5,100.0)	(99.658,100.0)	(99.613,100.0)	(99.593,100.0)
(99.5,101.0)	(99.639,101.0)	(99.604,101.0)	(99.583,101.0)
(99.5,102.0)	(99.627,102.0)	(99.593,102.0)	(99.572,102.0)
(99.5,103.0)	(99.625,103.0)	(99.591,103.0)	(99.571,103.0)
(99.5,104.0)	(99.625,104.0)	(99.592,104.0)	(99.572,104.0)

manually draw a 256 × 256 black and white image as shown in Fig. 16, where the pixel gray value in the 100th to 156th row and 100th to 156th column of the image is 1, and the background is 0, the sub-pixel edge coordinates extracted by different detection algorithms are shown in Table 1.

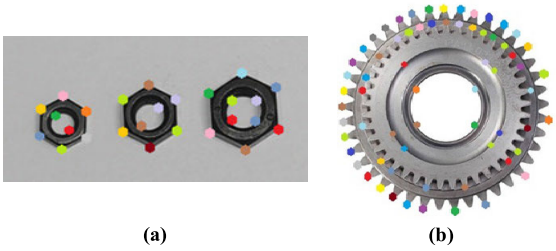

FIGURE 17. Two component images and the sub-pixel edge position. (a) screw and (b) gear.

In addition, edge detection of two different part images (as shown in Fig. 17) were compared using Visionpro 8.2 software (Cognex Corp., Natick, MA, USA) and the proposed interpolation algorithm. The detected sub-pixel edge coordinates are shown in the table 2 and 3.

2) COMPARATIVE ANALYSIS OF DETECTION EFFICIENCY

The main factors affecting the operating speed of algorithms are the principle and the optimization of the algorithm program. Matlabpool instructions were used to accelerate computing speed, so that it can run faster on a 4-core CPU. In this experiment, four images with different edge contour complexity were selected to test detection efficiency, as shown in Fig.18. The experimental results are shown in Fig.19. it can be seen that the proposed algorithm has higher detection efficiency than Canny-Steger and Canny/Devernay. Although

TABLE 2. Part image (a) sub-pixel edge coordinate.

Visionpro 8.2	Canny	Interpolate three points
(31.359,60.596)	(31.526,60.637)	(31.421,60.612)
(49.635,50.357)	(49.732,50.293)	(49.695,50.329)
(98.568,54.254)	(98.648,54.275)	(98.597,54.261)
(118.351,40.365)	(118.218,40.415)	(118.337,40.384)
(169.267,48.459)	(169.218,48.601)	(169.245,48.547)

TABLE 3. Part image (b) sub-pixel edge coordinate.

Visionpro 8.2	Canny	Interpolate three points
(156.185,23.378)	(156.258,23.319)	(156.205,23.357)
(172.573,29.354)	(172.651,29.394)	(172.597,29.372)
(187.751,37.172)	(187.637,37.196)	(187.735,37.181)
(200.851,48.364)	(200.784,48.394)	(200.835,48.375)
(211.713,60.462)	(211.769,60.501)	(211.729,60.483)

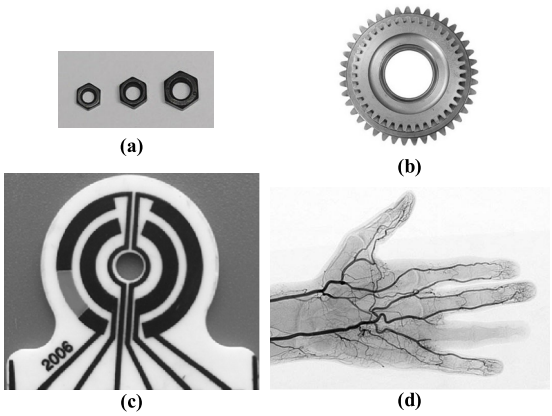

FIGURE 18. Four images with different pixel sizes and edge complexity used in detection efficiency comparison. (a) screw, (b) gear, (c) ceramic substrate thick film printing resistor, and (d) Blood vessel X-ray image.

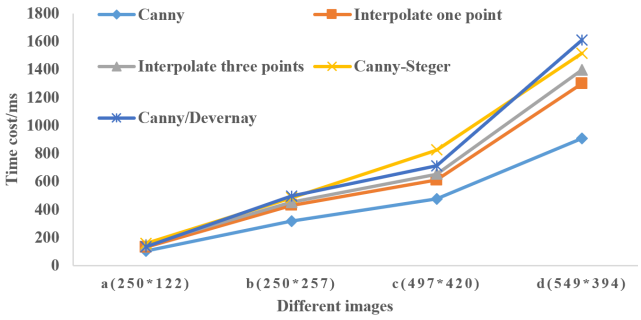

FIGURE 19. Detection efficiency comparison.

interpolating one point is faster than interpolating three points, the smoothness of interpolating one point is a little worse. Visual observation showed that interpolation of five

points cannot improve the smoothness of contour significantly, however it increased the calculation time. Therefore, three points interpolation method was selected in detecting the contour of ceramic substrate thick film printing resistor.

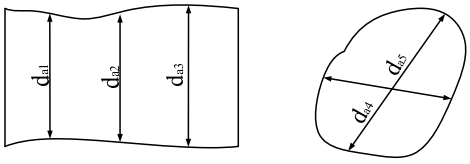

FIGURE 20. Cases of a single dimension have multi measured values.

C. ANALYSIS OF ERROR

Errors are typically considered the differences between the measured values and actual values, but a single dimension contains many true values [33] For example, the true diameter of an axle as shown in Fig. 20 includes d_{a1}, d_{a2},..., and d_{a5}, etc. Due to the uncertainty of the true value, it is difficult to determine the measurement error by analyzing the relationship between the measured results and the true values. Errors can include random error, systematic error, and careless error. Random error is caused by random factors in the measurement process, such as vibration, fluctuation, visual error and similar processes. Random error is normally distributed. For a given measurement condition, the numerical value and symbol of the systematic error state should be unchanged, or be distributed with regularity. Careless error is error beyond the expected error under certain conditions. In this subsection we will analyze the systematic error caused by this algorithm.

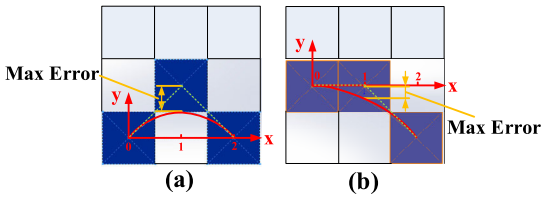

FIGURE 21. The cartesian coordinates of interpolated points for V-type and L-type edge pixels arrangement modes.

To analyze the systematic error, it is assumed that the center of the pixel is exactly at the edge of the measured element. Based on this assumption, for the symmetrically arranged linear edge pixels, this method can obtain the exact edge. For other directions or other shapes, the edges are considered to include a series of smooth curves. When the curvature of edge increases, the systematic error will increase. The representative V-type and L-type edge pixels arrangement modes were chosen to establish a reasonable coordinate system for error analysis. Fig. 21 shows the standard coordinate system for these two pixel arrangement modes. In order to obtain more accurate error accuracy, we have brought 10 interpolation points in a single pixel range, and brought a total of 20 sub-pixel interpolation points in these two pixel arrange modes. TABLE 4 shows both the original positions and interpolated positions. For V-type edge pixel arrangement modes, the max systematic error is 0.5 pixel, and for L-type edge pixel arrangement modes, the max systematic error is 0.25 pixel.

TABLE 4. The original value and interpolated value of sub-pixel points for V-type and L-type edge pixels arrangement modes.

Point	x	V Type original value	L Type original value	V Type interpolated value	L Type interpolated value	V Type error	L Type error
0	0	0	0	0	0	0	0
1	0.1	0.1	0	0.095	-0.0025	0.005	0.0025
2	0.2	0.2	0	0.18	-0.01	0.02	0.01
3	0.3	0.3	0	0.255	-0.0255	0.045	0.0255
4	0.4	0.4	0	0.32	-0.04	0.08	0.04
5	0.5	0.5	0	0.375	-0.0625	0.125	0.0625
6	0.6	0.6	0	0.42	-0.09	0.18	0.09
7	0.7	0.7	0	0.455	-0.1225	0.245	0.1225
8	0.8	0.8	0	0.48	-0.16	0.32	0.16
9	0.9	0.9	0	0.495	-0.2025	0.405	0.2025
10	1	1	0	0.5	-0.25	0.5	0.25
11	1.1	0.9	-0.1	0.495	-0.3025	0.405	0.2025
12	1.2	0.8	-0.2	0.48	-0.36	0.32	0.16
13	1.3	0.7	-0.3	0.455	-0.4225	0.245	0.1225
14	1.4	0.6	-0.4	0.42	-0.49	0.18	0.09
15	1.5	0.5	-0.5	0.375	-0.5625	0.125	0.0625
16	1.6	0.4	-0.6	0.32	-0.64	0.08	0.04
17	1.7	0.3	-0.7	0.255	-0.7225	0.045	0.0225
18	1.8	0.2	-0.8	0.18	-0.81	0.02	0.01
19	1.9	0.1	-0.9	0.095	-0.9025	0.005	0.0025
20	2	0	-1	0	-1	0	0

IV. CONCLUSION

In this paper, we presented a sub-pixel precision contour extracting algorithm for ceramic substrate thick film printing resistor measurement. In this method, through the mapping principle of R, G and B three-dimensional space cartesian coordinate system, the coordinate value of RGB pixel is projected on the space line of R=G=B to obtain gray image, pixel edges are located using a Canny detector, the edge width is thinned to a single pixel by morphological thinning, and sub-pixel contours are extracted using interpolation. In the sub-pixel level contour extraction process, a Single-Pixel-Multi-Point interpolation method was developed to enhance contour smoothness and achieve high precision for edge feature estimation. That method divides edge pixels in a 3×3 pixels block into nine arrangement modes, with one for a single-pixel edge, two for two-pixel edges, three for three-pixel edges, two for four-pixel edges, and one for five-pixel edge. According to the arrangement of the eight neighborhood edge pixels of the centered-edge pixel, the coordinates of interpolated sub-pixel points were calculated by interpolation with Bezier curves.

The systematic error of this method was analyzed by assuming that the center of the edge pixel is exactly at the edge of the measured element. For the symmetrically linear aligning edge pixels, this method can obtain the exact contour. As the curvature of edge increases, the error will increase. For V-type edge pixel arrangement modes, the max systematic

error is 0.5 pixel, and for L-type edge pixel arrangement modes, the max systematic error is 0.25 pixel.

REFERENCES

[1] M. H. Hueckel, "A local visual operator which recognizes edges and lines," *J. ACM*, vol. 20, no. 4, pp. 634–647, Oct. 1973.

[2] A. J. Tabatabai and O. R. Mitchell, "Edge location to subpixel values in digital imagery," *IEEE Trans. Pattern Anal. Mach. Intell.*, vol. PAMI-6, no. 2, pp. 188–201, Mar. 1984.

[3] E. P. Lyvers, O. R. Mitchell, M. L. Akey, and A. P. Reeves, "Subpixel measurements using a moment-based edge operator," *IEEE Trans. Pattern Anal. Mach. Intell.*, vol. 11, no. 12, pp. 1293–1309, Dec. 1989.

[4] S. Ghosal and R. Mehrotra, "Orthogonal moment operators for subpixel edge detection," *Pattern Recognit.*, vol. 26, no. 2, pp. 295–306, Feb. 1993.

[5] A. Trujillo-Pino, K. Krissian, M. Alemán-Flores, and D. Santana-Cedrés, "Accurate subpixel edge location based on partial area effect," *Image Vis. Comput.*, vol. 31, no. 1, pp. 72–90, Jan. 2013.

[6] M. K. Balasundaram and M. M. Ratnam, "In-process measurement of surface roughness using machine vision with sub-pixel edge detection in finish turning," *Int. J. Precis. Eng. Manuf.*, vol. 15, no. 11, pp. 2239–2249, Nov. 2014.

[7] D. Adapa, A. N. J. Raj, S. N. Alisetti, Z. Zhuang, K. Ganesan, and G. Naik, "A supervised blood vessel segmentation technique for digital fundus images using Zernike moment based features," *PLoS ONE*, vol. 15, no. 3, Mar. 2020, Art. no. e0229831.

[8] Q. Ying-Dong, C. Cheng-Song, C. San-Ben, and L. Jin-Quan, "A fast subpixel edge detection method using Sobel–Zernike moments operator," *Image Vis. Comput.*, vol. 23, no. 1, pp. 11–17, Jan. 2005.

[9] X. Xie, S. Ge, M. Xie, F. Hu, and N. Jiang, "An improved industrial sub-pixel edge detection algorithm based on coarse and precise location," *J. Ambient Intell. Hum. Comput.*, vol. 11, no. 5, pp. 2061–2070, May 2020.

[10] Q. Wang, C. Zhang, and P. M. Atkinson, "Sub-pixel mapping with point constraints," *Remote Sens. Environ.*, vol. 244, Jul. 2020, Art. no. 111817.

[11] J. H. Lee, T.-W. Kim, D. H. Ku, and H. J. Pahk, "Active contour method based sub-pixel critical dimension measurement of thin film transistor liquid crystal display (TFT-LCD) patterns," *Int. J. Precis. Eng. Manuf.*, vol. 21, no. 5, pp. 831–841, May 2020.

[12] A. Kaur and C. Sing, "Sub-pixel edge detection using pseudo Zernike moment," *Int. J. Signal Process., Image Process. Pattern Recognit.*, vol. 4, no. 2, pp. 107–118, 2011.

[13] B. Z. Wei and Z. M. Zhao, "A sub-pixel edge detection algorithm based on Zernike moments," *Imag. Sci. J.*, vol. 61, no. 5, pp. 436–446, Jun. 2013.

[14] Q. Sun, Y. Hou, Q. Tan, C. Li, and M. Liu, "A robust edge detection method with sub-pixel accuracy," *Optik, Int. J. Light Electron Opt.*, vol. 125, no. 14, pp. 3449–3453, Jul. 2014.

[15] Q. Sun, Y. Hou, and Q. Tan, "A subpixel edge detection method based on an arctangent edge model," *Optik*, vol. 127, no. 14, pp. 5702–5710, Jul. 2016.

[16] G. Wang, "A sub-pixel circle detection algorithm combined with improved RHT and fitting," *Multimedia Tools Appl.*, vol. 79, nos. 39–40, pp. 29825–29843, Oct. 2020.

[17] Z. Wei, M. Zhao, and Y. Tong, *Sub-Pixel Edge Detection Algorithm Based on the Fitting of Gray Gradient and Hyperbolic Tangent Function*. Cham, Switzerland: Springer, 2014, pp. 287–294.

[18] L. Xuan and Z. Hong, "An improved canny edge detection algorithm," in *Proc. 8th IEEE Int. Conf. Softw. Eng. Service Sci. (ICSESS)*, Nov. 2017, pp. 275–278.

[19] K. Jensen and D. Anastassiou, "Subpixel edge localization and the interpolation of still images," *IEEE Trans. Image Process.*, vol. 4, no. 3, pp. 285–295, Mar. 1995.

[20] T. Hermosilla, E. Bermejo, A. Balaguer, and L. A. Ruiz, "Non-linear fourth-order image interpolation for subpixel edge detection and localization," *Image Vis. Comput.*, vol. 26, no. 9, pp. 1240–1248, Sep. 2008.

[21] L. Pap and J. J. Zou, "Sub-pixel edge detection for photogrammetry using laplace difference of Gaussian and 4th order ENO interpolation," in *Proc. IEEE Int. Conf. Image Process.*, Sep. 2010, pp. 2841–2844.

[22] X. C. Shi, Z. Z. Sun, and S. L. Lu, "A novel method of sub-pixel linear edge detection based on first derivative approach," *Adv. Mater. Res.*, vols. 139–141, pp. 2107–2111, Oct. 2010.

[23] Y. Chen, Y. Li, and Y. Zhao, "Sub-pixel detection algorithm based on cubic B-spline curve and multi-scale adaptive wavelet transform," *Optik*, vol. 127, no. 1, pp. 11–14, Jan. 2016.

[24] J. Sánchez, "Comparison of motion smoothing strategies for video stabilization using parametric models," *Image Process. Line*, vol. 7, pp. 309–346, Nov. 2017.

[25] C. Steger, M. Ulrich, and C. Wiedemann, *Machine Vision Algorithms and Applications*. Hoboken, NJ, USA: Wiley, 2008.

[26] J. Canny, "A computational approach to edge detection," *IEEE Trans. Pattern Anal. Mach. Intell.*, vol. PAMI-8, no. 6, pp. 679–698, Nov. 1986.

[27] B. Jähne, H. Scharr, and S. Körkel, *Handbook of Computer Vision and Applications*. New York, NY, USA: Academic, 1999.

[28] M. Hazewinkel, *Encyclopedia of Mathematics*. London, U.K.: Springer, 2001.

[29] L. S. Davis, "A survey of edge detection techniques," *Comput. Graph. Image Process.*, vol. 4, no. 3, pp. 248–260, Sep. 1975.

[30] J. M. S. Prewitt, "Object enhancement and extraction," in *Picture Processing and Psychopictorics*. New York, NY, USA: Academic, 1970.

[31] D. Marr and E. Hildreth, "Theory of edge detection," *Proc. Roy. Soc. London. B, Biol. Sci.*, vol. 207, no. 1167, pp. 187–217, 1980.

[32] P. E. Bézier, *Essai De Définition Numérique Des Courbes Et Des Surfaces Expérimentales*. Paris, France: Université Pierre et Marie Curie, 1977.

[33] F. L. Hu, *Interchangeability and Technical Measurement Basis*. Beijing, China: Higher Education Press, 2010.

TIAN-HU LIU was born in Ganzhou, Jiangxi, China, in 1974. He received the B.S. degree in engine engineering from Jilin University, Changchun, Jilin, China, in 1996, and the M.S. degree in material process engineering and the Ph.D. degree in mechanical and electronic engineering from the Guangdong University of Technology, Guangzhou, Guangdong, China, in 2002 and 2006, respectively.

From 1996 to 1999, he was an Assistant Engineer with Jiangling Motors Company Ltd. From 2002 to 2003, he was an Assistant Engineer with the Dongguan Quality Supervision and Inspection Institute. From 2007 to 2010, he was an Assistant Professor with the College of Engineering, South China Agricultural University, Guangzhou, where he has been an Associate Professor, since 2010. He is the author of more than 40 articles and holds more than ten patents. His research interests include computer vision, robotics, and precision agriculture.

GUI-QI LI was born in Nanjing, Jiangsu, China, in 1992. He received the B.S. degree in automation from the Tongda College, Nanjing University of Posts and Telecommunications, Nanjing, in 2018. He is currently pursuing the master's degree with the College of Engineering, South China Agricultural University, Guangzhou, Guangdong, China.

His research interests include visual recognition, deep learning, image recognition, mechanical design, intelligent agricultural equipment, and precision agriculture.

XIANG-NING NIE was born in Longhui, Hunan, China, in 1998. She received the B.S. degree in electronic information from the Hunan University of Arts and Science, Hunan, in 2019. She is currently pursuing the master's degree with the College of Engineering, South China Agricultural University, Guangzhou, Guangdong, China.

Her research interests include visual recognition, deep learning, image recognition, mechanical design, and industrial robotics.

HONG-JUN WANG was born in Chongqing, China, in 1966. She received the B.S. degree from Chongqing University, Chongqing, in 1987, the M.S. degree from the University of Electronic Science and Technology, Chengdu, Sichuan, China, in 1994, and the Ph.D. degree in mechanical and electronic engineering from the Guangdong University of Technology, Guangzhou, Guangdong, China, in 2003.

From 2003 to 2013, she was an Associate Professor with the College of Engineering, South China Agricultural University, where she has been a Professor, since 2013. She is the author of more than 40 articles and holds more than ten inventions. Her research interests include intelligent agriculture, machine vision, robotics, and intelligent design.

DI ZHANG was born in Lianyungang, Jiangsu, China, in 1997. She received the B.S. degree in automation from the Nanjing University of Information Science and Technology, Nangjing, Jiangsu, in 2019. She is currently pursuing the master's degree with the College of Engineering, South China Agricultural University, Guangzhou, Guangdong, China.

Her research interests include visual recognition, deep learning, automation, image recognition, communication, and precision agriculture.

JIN-MENG WU was born in Xinyang, Henan, China, in 1997. She received the B.S. degree in network engineering from the Hunan University of Technology, in 2018. She is currently pursuing the master's degree with the College of Engineering, South China Agricultural University, Guangzhou, Guangdong, China.

Her research interests include image processing, deep learning, and computer vision.

WEI LIU was born in Xinhua, Hunan, China, in 1998. He received the B.S. degree in mechanic engineering and automation from Jishou College, Jishou, Hunan, in 2020. He is currently pursuing the master's degree with the College of Engineering, South China Agricultural University, Guangzhou, Guangdong, China.

His research interests include computer vision, mechanical design, automation, mechanical motion simulation, and intelligent agriculture.